sustainability

MDPI

Article

Waste-to-Resource Conversion of Cow Dung Ash for Sustainable Wastewater Treatment: Isotherm Modeling and MOORA Evaluation

Vaibhav R. Chate [1], Nitin A. Deshpande [1], Raviraj M. Kulkarni [2], Ganesh R. Chate [3,*], Yunus Shukor [4] and Manjunath Shettar [5,*]

1 Department of Civil Engineering, K.L.S. Gogte Institute of Technology, Visvesvaraya Technological University, Belagavi 590008, Karnataka, India
2 Department of Chemistry, Jain College of Engineering and Research, Visvesvaraya Technological University, Belagavi 590008, Karnataka, India
3 Department of Mechanical Engineering, K.L.S. Gogte Institute of Technology, Visvesvaraya Technological University, Belagavi 590008, Karnataka, India
4 Department of Biochemistry, Faculty of Biotechnology and Biomolecular Sciences, Universiti Putra Malaysia, Serdang 43400, Selangor, Malaysia
5 Manipal Institute of Technology, Manipal Academy of Higher Education, Manipal 576104, Karnataka, India
* Correspondence: ganeshchate@git.edu (G.R.C.); manjunath.shettar@manipal.edu (M.S.)

Abstract

Low-cost adsorbents derived from agricultural and livestock waste offer a sustainable approach to wastewater remediation. In this study, a material derived from cow dung ash (SMCDA) was prepared through a simple waste-valorization route without chemical activation and evaluated for the removal of methylene blue (MB) from aqueous solution. X-ray diffraction, Fourier-transform infrared spectroscopy, scanning electron microscopy, energy-dispersive X-ray spectroscopy, Brunauer–Emmett–Teller analysis, and zeta-potential measurements were used to characterize the mineral composition, surface functional groups, morphology, pore structure, and surface charge of SMCDA. Batch adsorption experiments examined the effects of solution pH, adsorbent dosage, initial MB concentration, contact time, and temperature. The highest removal efficiency, 97.33%, was obtained at pH 8 with an SMCDA dosage of 1000 mg L^{-1}. Equilibrium data were fitted using seven isotherm models and evaluated using multiple statistical criteria and Multi-Objective Optimization by Ratio Analysis (MOORA). The Freundlich model achieved the highest MOORA ranking and predicted an equilibrium adsorption capacity of 13.944 mg g^{-1} at the highest concentration investigated, which is close to the experimental value of 14.425 mg g^{-1}. The results are consistent with heterogeneous adsorption involving electrostatic attraction, possible π–π interactions, hydrogen bonding, and pore filling. These findings demonstrate the potential of cow dung ash as a low-cost adsorbent prepared without hazardous chemical activating agents.

Keywords: cow dung valorization; sustainable wastewater treatment; biomass-derived adsorbent; methylene blue adsorption; water pollution remediation; MOORA; clean water technologies

Check for updates

Academic Editors: Giovanni De Feo and Malgorzata Kacprzak

Received: 6 June 2026
Revised: 6 August 2026
Accepted: 11 August 2026
Published: 13 August 2026

Copyright: © 2026 by the authors. Licensee MDPI, Basel, Switzerland. This article is an open access article distributed under the terms and conditions of the Creative Commons Attribution (CC BY) license.

1. Introduction

Many industries use dyes to color goods, along with large volumes of water, resulting in the discharge of substantial volumes of colored wastewater [1]. Organic dyes can persist

and accumulate in the environment because they are non-biodegradable. Globally, over 0.70 million tonnes of dyes are produced, out of which up to 15% may be released into aquatic environments [2]. Due to their complex and stable chemical structures, dyes pose serious environmental risks and are challenging to treat [3,4]. Due to stringent restrictions, it is essential to remove dyes and other colorants from industrial effluents prior to disposal [5–7]. A prominent dye compound with numerous industrial applications is methylene blue (MB). MB is a well-known cationic dye contaminant due to its possible adverse effects on aquatic organisms, ecosystems, and human health [8–10]. Several approaches are employed to remediate dye wastewater, including sorption, membrane separation, oxidation/ozonation, anaerobic/aerobic treatment, and coagulation/flocculation [11–13]. Adsorption is one of the most widely used physicochemical treatment methods [14–17]. Worldwide biomass generation is predicted to surpass 130 billion tonnes per year [18–20]. Biomass, a sustainable resource, is employed for water treatment. Many adsorbents are employed to remove MB (Table 1). To address the underutilization of livestock manure in wastewater treatment, this study examines cow dung as an alternative biosorbent for MB removal. The approach employed to synthesize SMCDA is straightforward and delivers competitive adsorption performance, in contrast to typical activated adsorbents that require high-energy or intensive chemical processing.

Table 1. Comparison of MB removal using different adsorbents.

Adsorbent Material	MB Adsorption Capacity (mg g^{-1})	Reference	Key Sustainability Feature
Rice husk ash (RHA)	8.59	[1]	Silica-rich ash
Low-temperature cattle manure biochar	20–25	[21]	Low-energy biochar production from animal manure
Rice husk	24.48	[22]	Lignocellulosic, biogenic silica (SiO_2)
Bagasese-based materials	41	[23]	Lignocellulosic sorbent
Acid-treated cow dung (TCD)	64.26	[24]	Enhanced adsorption via acid activation
SMCDA	13.944	Present study	Chemical-free transformation of cow dung into a mesoporous adsorbent.

In the present study, a sustainable hierarchical nanoporous material synthesized from cow dung ash (SMCDA) particles is produced by the combustion of cow dung cakes with rice and ghee. The utilization of SMCDA as an adsorbent is a waste-to-resource process, in which a low-commercial-value residue, cow dung ash, is transformed into a functional material for MB removal. The present approach may alleviate the burden of livestock waste disposal to the environment and offer a low-cost adsorbent for wastewater treatment. Preparation of SMCDA is simple and does not require intensive chemical modification as compared to many chemically activated adsorbents. Thus, the process is potentially attractive from a sustainable-treatment perspective. Energy-dispersive X-ray spectroscopy, FTIR, scanning electron microscopy, Brunauer–Emmett–Teller (BET), Zeta potential, and X-ray diffraction are used to evaluate the nanoporous materials produced from SMCDA. This study supports the view that nanoporous materials from SMCDA can adsorb MB from aqueous solutions. Temperature, pH, SMCDA dosage, adsorption time, kinetics, and the results of initial MB concentration are also examined. Seven Isotherm models are evaluated. The MOORA is adopted to select the optimal adsorption isotherm model.

This study addresses waste management and water quality problems simultaneously by valorizing waste for wastewater treatment. The outcomes highlight SMCDA's potential as a sustainable adsorbent for environmental applications.

2. Materials and Methods

2.1. Materials

Cow dung is an affordable biomass source for producing an SMCDA adsorbent containing carbon, inorganic minerals, and lignocellulosic materials. It produces an adsorbent with active sites and porosity, ideal for adsorbing MB from water after processing with rice and ghee (ratio of Cow dung:rice:ghee = 86.2:3.5:10.3 by mass). MB is used as a model cationic dye without further purification; it is purchased from Sigma-Aldrich. Its molecular weight is 319.85 g mol^{-1}, and its molecular formula is $C_{16}H_{18}ClN_3S$. Because of its low pK_a (~3.8), MB is an aromatic heterocyclic compound that predominantly exists in its positively charged state in aqueous solutions across a wide pH range. Due to its high stability and extensive use in the textile and dyeing sectors, MB is frequently considered a typical pollutant for assessing the adsorption capabilities of materials. All aqueous solutions are prepared using deionized water.

2.2. Methodology

2.2.1. Preparation of SMCDA

The materials required to prepare SMCDA are copper vessels, dried cow dung (50 g), cow's ghee, and rice. For preparation, the semi-pyramidal copper vessel is placed, then two small cow dung cubes are placed at the bottom, with one on top of the other to allow for good airflow. The flame is ignited between the cow dung cubes. A total of 2 g of rice is divided into 2 parts and added to the vessel. Then, 6 g of cow's ghee is slowly added to the vessel using a wooden spoon. Combustion is allowed to continue for 30 min, after which the flame is extinguished. The initial temperature reaches 500 °C upon ignition, then ranges from 750 °C to 800 °C and thereafter decreases to 600 °C during synthesis. The formed ash is cooled, crushed, and sieved through a 75 µm mesh to obtain SMCDA. To reduce reagent usage, processing steps, and the production of residual hazardous chemicals, the synthesis is carefully planned to eliminate chemical activation. The zeta potential of SMCDA (Nano ZS90, Malvern, UK) is then measured in deionized water as the dispersant, without any supporting electrolyte or pH adjustment. BET analysis (BELSORP-mini II analyser, Microtrac MRB, Osaka, Japan) of SMCDA is performed using Nitrogen (N_2) as the adsorption gas, and the adsorption–desorption isotherms are recorded at 77 K. The pore-size distribution is determined using the Barrett–Joyner–Halenda (BJH) method. The degassing is performed at 200 °C for 2 h.

2.2.2. Adsorption Experiment

A known quantity (50 mL) of MB and SMCDA is employed in a batch experiment on a magnetic stirrer at room temperature (25 °C) to investigate the adsorption of MB. All the solutions after adsorption are centrifuged (14000 rpm for 12 min) and examined in a UV-visible spectrophotometer at 665 nm (Agilent Cary 60, Santa Clara, CA, USA) after calibrating the instrument for initial MB concentrations ranging from 10 µM to 50 µM. Adsorption experiments are conducted at the optimal stirring speed of 700 rpm, with initial MB concentrations ranging from 15 µM to 50 µM and SMCDA dosages ranging from 100 to 1000 mg L^{-1}. pH of the MB aliquot is set using HCl and NaOH solutions. The pH of each solution is measured with a pH meter (HACH, Loveland, CO, USA) prior to the addition of the SMCDA dosage. The equilibrium time for adsorption is 4 h. The average of three replicates is used in subsequent calculations.

The removal efficiency (%) and equilibrium adsorption capacity (q_e) (mg g^{-1}) are calculated using the following equations:

$$\text{Removal efficiency}(\%) = \frac{(M_0 - M_e)}{M_0} \times 100 \quad (1)$$

$$q_e\left(\text{mg g}^{-1}\right) = \frac{(M_0 - M_e) \times \text{molecular weight of MB} \times 10^{-3} \times V}{m} \quad (2)$$

where M_0 = initial MB concentration (μM), M_e = equilibrium MB concentration (μM), V = solution volume (L), and m = mass of the SMCDA (g). These equations are used to quantify the adsorption performance under equilibrium conditions.

Note: Error bars represent the standard deviation of triplicate measurements.

2.2.3. Adsorption Kinetic Modeling

MB solution (15 μM) at neutral pH, with an SMCDA dosage of 1000 mg L^{-1}, is employed for the kinetic study at various time intervals (0.5 to 4 h). The kinetic adsorption data are analyzed using both pseudo-first-order (PFO) and pseudo-second-order (PSO) models. The pseudo-first-order model suggests that the rate of adsorption is proportional to the difference between the equilibrium adsorption capacity and the adsorption capacity at contact time. The pseudo-second-order model is based on the assumption that the rate of adsorption is proportional to the square of the difference. Both models are assessed by nonlinear regression and statistical indicators [25]. The pseudo-second-order model fits the experimental data better than the pseudo-first-order model under the conditions used in the present study, and the adsorption rate of MB is better described by the pseudo-second-order model (Tables S1 and S2).

Equation for nonlinear PFO:

$$q_t = q_e\left(1 - e^{-k_1 t}\right) \quad (3)$$

Equation for nonlinear PSO:

$$q_t = \frac{k_2 q_e^2 t}{(1 + k_2 q_e t)} \quad (4)$$

Marquardt's Percent Standard Deviation (MPSD) is a statistical tool used to assess how well a mathematical model fits experimental data.

$$\text{MPSD} = 100\sqrt{\left(\frac{1}{n-p}\right)\sum_{i=1}^{n}\left(\frac{q_{t,i,\text{exp}} - q_{t,i,\text{calc}}}{q_{t,i,\text{exp}}}\right)^2} \quad (5)$$

where q_t = adsorption capacity at time t (mg g^{-1}), q_e = equilibrium adsorption capacity (mg g^{-1}) k_1 = rate constant (h^{-1}) related to PFO, k_2 = rate constant (g mg^{-1} h^{-1}) related to PSO, t = contact time (h).

2.2.4. Adsorption Isotherm Modeling

The primary adsorption principles commonly applied in solid–liquid sorption processes are illustrated by the seven selected models, which have been thoroughly examined in prior research. The Langmuir, Freundlich, Temkin, Jovanovic, Sips, Toth, and Unilan isotherm models collectively represent homogeneous, heterogeneous, monolayer, multilayer, and hybrid adsorption mechanisms, accompanied by various adsorption energy distributions. They are used to analyze the adsorption equilibrium. When used together, they provide for a thorough and trustworthy evaluation of the adsorbent's surface proper-

ties and adsorption behavior across the concentration range under investigation. These models accurately represent the main adsorption mechanisms expected for MB adsorption by SMCDA; however, incorporating additional isotherms will provide valuable new perspectives and may lead to redundant model evaluations. Consequently, seven isotherm models are considered adequate for a thorough assessment of adsorption equilibrium characteristics (Table 2). The selected isotherm models represent different possible adsorption behaviors, monolayer adsorption, heterogeneous surface adsorption, and hybrid Langmuir–Freundlich behaviour. The model equations and parameter meanings are provided for clear comparison and reproducibility. Model selection is based on statistical fit, simplicity, parameter meaning, and physical plausibility. In order to execute the adsorption studies, 50 mg of SMCDA is added to various concentrations of MB solution (15 µM to 50 µM, solution volume = 50 mL) at equilibrium time (4 h) under neutral conditions. The details of q_e as per experimental conditions and predicted (by selected isotherm models) are presented in Table S3.

Table 2. Details of isotherm models and associated parameters.

Isotherm Model	p	Nonlinear Formula	Parameters and Units	Ref.	
Langmuir	2	$q_e = \frac{q_{mL} b_L C_e}{1+b_L C_e}$	q_{mL}: maximum monolayer adsorption capacity, mg g^{-1}; b_L: Langmuir affinity constant, L mg^{-1}.	[26]	(6)
Jovanovic	2	$q_e = q_{mJ}\left(1 - e^{-K_J C_e}\right)$	q_{mJ}: maximum adsorption capacity, mg g^{-1} K_J: Jovanovic adsorption constant, L mg^{-1}.	[27]	(7)
Freundlich	2	$q_e = K_F C_e^{1/n_F}$	K_F: Freundlich adsorption-capacity constant, $\left(\text{mg g}^{-1}\right)\left(\text{L mg}^{-1}\right)^{1/n_F}$; n_F: adsorption-intensity or surface-heterogeneity factor, dimensionless.	[28]	(8)
Temkin	2	$q_e = \frac{RT}{b_T}\ln(a_T C_e)$	a_T: equilibrium-binding constant, L mg^{-1}; b_T: constant related to the heat of adsorption, J mol^{-1} (mg g^{-1})$^{-1}$; R: universal gas constant, J mol^{-1} K^{-1}; T: absolute temperature, K.	[29]	(9)
Sips	3	$q_e = \frac{K_S q_{mS} C_e^{1/n_S}}{1+K_S C_e^{1/n_S}}$	q_{mS}: maximum adsorption capacity, mg g^{-1}; K_S: Sips affinity constant, $\left(\text{L mg}^{-1}\right)^{1/n_S}$; n_S: surface-heterogeneity parameter, dimensionless.	[30]	(10)
Toth	3	$q_e = \frac{q_{mT} K_T C_e}{\left[1+(K_T C_e)^{n_T}\right]^{1/n_T}}$	q_{mT}: maximum adsorption capacity, mg g^{-1}; K_T: Toth equilibrium constant, L mg^{-1}; n_T: surface-heterogeneity parameter, dimensionless.	[31]	(11)
Unilan	3	$q_e = \frac{q_{mU}}{2b_U}\ln\left(\frac{1+a_U C_e e^{b_U}}{1+a_U C_e e^{-b_U}}\right)$	q_{mU}: maximum adsorption capacity, mg g^{-1}; a_U: Unilan equilibrium constant, L mg^{-1}; b_U: adsorption-energy-distribution width parameter, dimensionless.	[32]	(12)

General parameters: q_e: equilibrium adsorption capacity, mg g^{-1}; C_e: equilibrium methylene-blue concentration in solution, mg L^{-1}; q_m: maximum adsorption capacity, mg g^{-1}; and p: number of adjustable model parameters, dimensionless.

2.3. Statistical Analysis

Various error function tests are utilized and include HQC (Hannan and Quinn's Criterion), Bias Factor (BF), Accuracy Factor (AF), root-mean-squared error (RMSE), coefficient of determination (R^2), corrected Akaike Information Criterion (AICc), and Bayesian Information Criterion (BIC) [33–37]. In general, n is the total number of observations, Ob_i and Pd_i are the observed and predicted values, and p is the number of adjustable model parameters [38,39].

RMSE is calculated using the following equation;

$$RMSE = \sqrt{\frac{\sum_{i=1}^{n}(Pd_i - Ob_i)^2}{n}} \quad (13)$$

BF and AF are calculated using the following equation;

$$Bias\ factor = 10^{\frac{1}{n}(\sum_{i=1}^{n} log_{10}(\frac{Pd_i}{Ob_i}))} \quad (14)$$

$$Accuracy\ factor = 10^{\frac{1}{n}(\sum_{i=1}^{n} |log_{10}(\frac{Pd_i}{Ob_i})|)} \quad (15)$$

AICc is calculated using the following equation;

$$AICc = 2p + nln\left(\frac{SSE}{n}\right) + \frac{2p(p+1)}{n-p-1} \quad (16)$$

BIC is calculated using the following equation;

$$BIC = nln\left(\frac{SSE}{n}\right) + pln(n) \quad (17)$$

HQC is calculated using the following equation;

$$HQC = nln\left(\frac{SSE}{n}\right) + 2pln(ln\ n) \quad (18)$$

Coefficient of determination (R^2) is calculated using the following equations;

$$R^2 = 1 - \frac{SSE}{(SST)} \quad (19)$$

$$SST = \sum_{i=1}^{n}(Ob_i - mean\ of\ observed\ values)^2 \quad (20)$$

$$SSE = \sum_{i=1}^{n}(Ob_i - Pd_i)^2 \quad (21)$$

2.4. Application of Multi-Objective Optimization by Ratio Analysis (MOORA) in Ranking Models

Since the best models typically have the highest consensus error function scores, the MOORA is used for multi-criteria decision-making (MCDM) in this modeling exercise [40–43]. By assessing various performance metrics concurrently, this method makes it easier to choose the best model. The use of MOORA, a subset of MCDM, for ranking adsorption isotherm models is first demonstrated by Shukor [44]. To ensure that various performance metrics are comparable, the decision matrix is normalized as the first

step in the methodology. Normalization is important because the units and magnitudes of these metrics can vary.

$$X'_{ij} = \frac{X_{ij}}{\sqrt{\sum_{i=1}^{m} X_{ij}^2}} \quad (22)$$

where X_{ij} = original value of the j^{th} metric for the i^{th} model, and X'_{ij} = normalized value.

Ratio System Analysis

Beneficial criteria are the error functions that should be maximized, R^2. On the other hand, non-beneficial criteria are error functions that should be minimized, which include the rest of the error functions. To reflect the relative importance of each function, weights are assigned. In this study, equal weights are attached to each normalized function and are then used to calculate the MOORA index following the equation:

$$Y_i = \sum_{j \in B} w_j X'_{ij} - \sum_{j \in NB} w_j X'_{ij} \quad (23)$$

where Y_i = MOORA index for the i^{th} model, B = beneficial criteria, NB = non-beneficial criteria, w_j = weight ($1/7 = 0.1428$).

The final step is the sorting of the models by their combined performance ratings. Higher scores signify better results. According to the specified decision criteria, the model with the highest value is deemed the best. The proposed approach provides a systematic and objective framework for comparing kinetic models and identifying the model that performs best across multiple evaluation criteria.

3. Results and Discussion

3.1. X-Ray Diffraction

The diffraction patterns are collected over a 2θ range of 10–80° using Cu Kα radiation (λ = 1.5406 Å). The XRD analysis of SMCDA (Figure 1) reveals several distinct diffraction peaks, indicating the presence of various mineral phases. The two 2θ peaks for the precursor route-prepared sample are identified at 22.73° (002 plane) and around 40.47° (101 plane), which are similar to those of the activated carbon samples. Sharp peaks are observed in SMCDA at 26.50^0 (101) and 68.24^0 (203), which are due to the presence of crystalline quartz as reported for similar peaks [45–48]. The plausibility that amorphous silica/ carbon is present is indicated with a peak at 21.92° (2θ) [49,50]. A diffraction peak at 29.78° is attributed to calcite ($CaCO_3$), indicating the presence of calcium species in SMCDA. Under the investigated pH conditions, calcite is chemically inert, and any residual calcium in the mixture, in various forms, is not released in sufficient quantities to augment adsorption [51]. Further, the literature also suggests that the peaks at 20.34° and 26.50° correspond to cow dung ash [52].

3.2. FTIR Analysis

The FTIR spectrum (using FTIR Spectrometer 4600, Jasco, Tokyo, Japan) of SMCDA (Figure 2) reveals several characteristic peaks. The absorption band centered at approximately 3500 cm^{-1} is attributed to the stretching vibration of hydroxyl (–OH) groups, indicating their presence on the adsorbent surface. The FTIR spectrum exhibits absorption bands in the range of 2885–2970 cm^{-1}, which are assigned to C–H stretching vibrations, while the band at 1440 cm^{-1} is associated with CH_2 bending (deformation) vibrations [46,47]. H_2O at 1656 cm^{-1}, Si–O–Si at 1095 cm^{-1} and 823 cm^{-1}, and Si-O at 480 cm^{-1} are consistent with the previous literature [50,53].

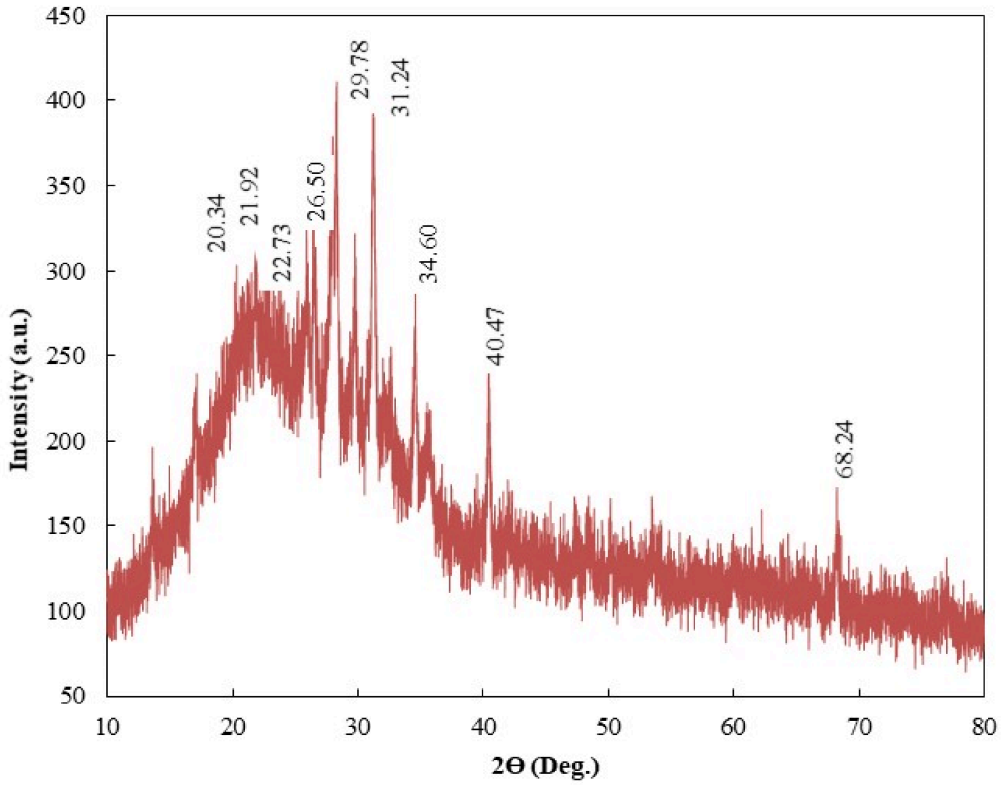


Figure 1. XRD analysis of SMCDA.

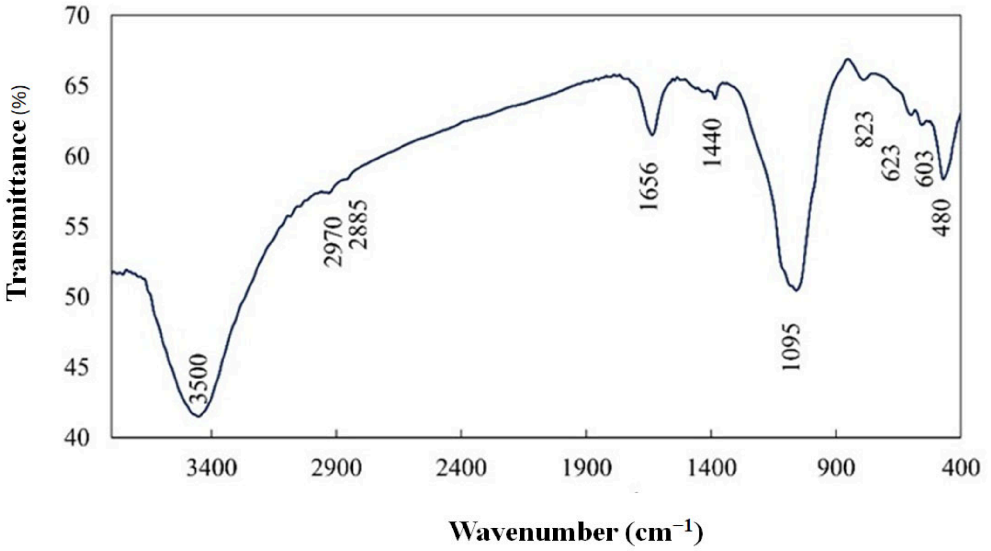


Figure 2. FTIR spectrum of SMCDA.

3.3. Energy-Dispersive X-Ray Spectroscopy [EDS]

The elemental composition of SMCDA is characterized using EDS, which confirms the presence of C, O, Al, Si, P, Mg, K, and Ca (Figure 3). The EDS results indicate that oxygen (47.01 wt%) and carbon (15.48 wt%) are the dominant constituents, implying that the material is primarily composed of oxide and/or carbonate phases. The high oxygen concentration suggests the presence of metal oxides (MgO, CaO, Al_2O_3, SiO_2), consistent with the occurrence of silicon (11.63%), magnesium (5.81%), and calcium (8.30%).

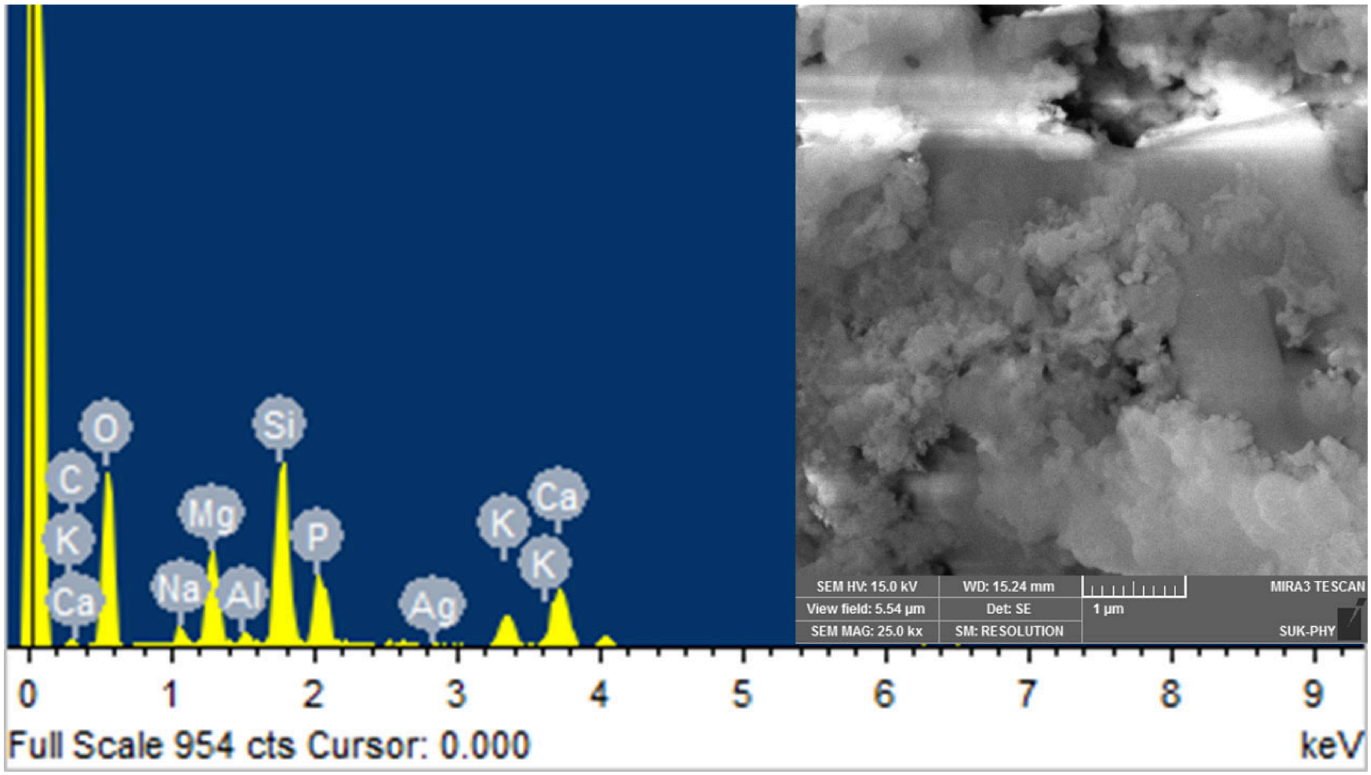


Figure 3. EDS spectrum of SMCDA (iInset SEM image).

3.4. Scanning Electron Microscopy

The SEM image of the SMCDA shows a rough and heterogeneous surface with many surface pores suitable for adsorption (Figure 3 (inset: SEM image)). SEM analysis is used only for qualitative assessment due to the imaging resolution (scale bar: 1 µm), and no quantitative interpretation of pore size is performed. Thus, SEM provides qualitative confirmation of morphology, while BET provides a quantitative basis for assessing pore structure.

3.5. Impact of MB Concentration at Different Adsorption Times

The initial concentration of MB significantly influences the removal efficiency, while keeping the SMCDA dosage (1000 mg L^{-1}) constant. The concentration of the synthetic solution varies from 15 µM to 50 µM. At 298 K, the removal efficiency decreases as the initial MB concentration increases (Figure 4). Upon adsorption, most binding sites on the SMCDA are initially available. However, as MB concentration increases, the SMCDA phase becomes saturated with MB, thereby decreasing removal efficiency.

3.6. Effect of SMCDA Dosage

MB solution (15 µM) at neutral pH and constant concentration is aliquoted, with SMCDA dosage ranging from 100 to 1000 mg L^{-1}, and stirred at 700 rpm for the equilibrium time before centrifugation. Figure 5 shows that the optimal SMCDA dosage for maximal MB adsorption is 1000 mg L^{-1}, as the MB removal efficiency between 900 and 1000 mg L^{-1} is marginal, indicating that most of the MB is removed and the removal efficiency approaches a plateau. The removal of MB is enhanced by increasing SMCDA dosage, due to more active adsorption sites and the presence of surface functional groups. Numerous active sites facilitate surface complexation, π–π interactions (plausible), and electrostatic interactions with MB molecules.

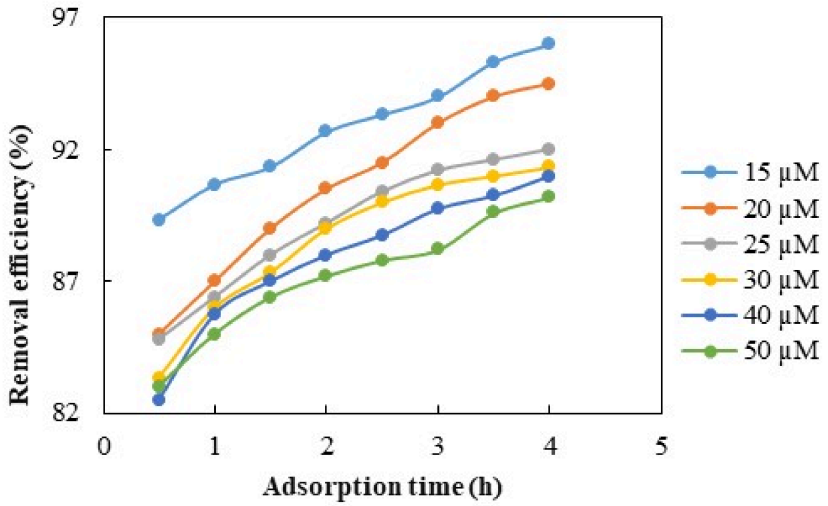


Figure 4. Effect of initial MB concentration at various adsorption time (Experimental conditions: dosage of SMCDA = 1000 mg L^{-1}, under natural pH condition, adsorption time = 4 h, including initial 0.5 h stirring at 700 rpm).

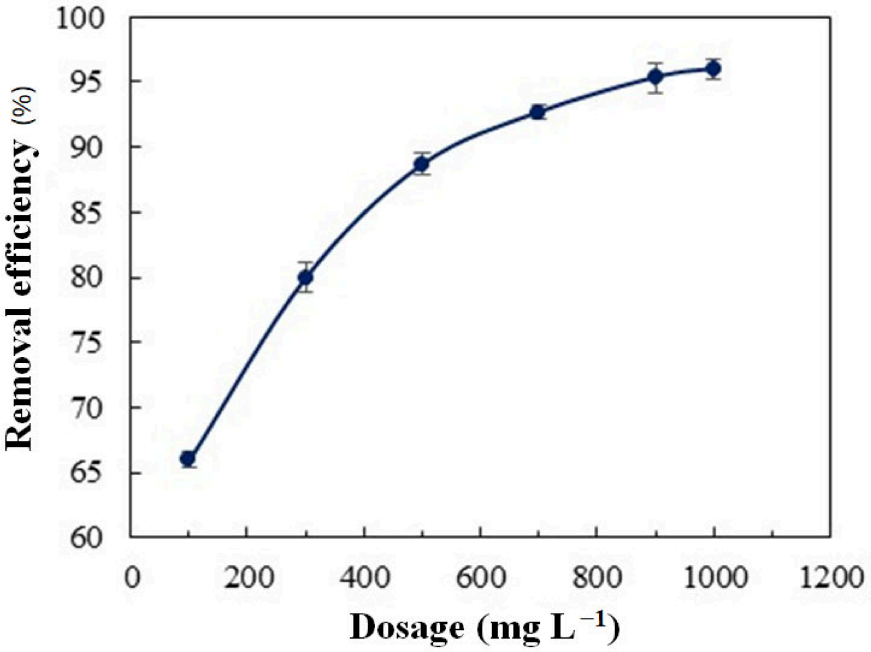


Figure 5. Influence of SMCDA dosage (Experimental conditions: initial MB concentration at neutral pH = 15 µM, adsorption time = 4 h, including initial 0.5 h stirring at 700 rpm).

3.7. Effect of pH on MB Removal by SMCDA

MB sorption by SMCDA is examined over a pH range of 3–9, with other parameters held constant (SMCDA 1000 mg L^{-1}, Initial MB 15 µM) at equilibrium. The reported pH_{pzc} values for cow dung and modified cow dung are 4.16 and 4.53, respectively [24]. The literature also suggests that thermal conversion products (biomass ashes) typically exhibit increased alkalinity due to the breakdown of acidic functional groups and the formation of alkaline mineral oxides [17]. The adsorption effectiveness improves at higher pH values (pH > 7), suggesting that alkaline conditions are advantageous for MB removal. Under alkaline conditions, the removal efficiency gradually increases, reaching a maximum of 97.33% at pH 8 and remaining nearly constant at pH 9 (Figure 6). The favorable electrostatic interaction between the MB (+ve) and SMCDA (-ve) sites is agreeable for this enhancement.

Surface protonation and subsequent electrostatic repulsion are consistent with the decreased adsorption observed in acidic environments. The ideal pH range of 8–9 indicates that pH-dependent surface charge interactions strongly govern adsorption. Adsorption is further influenced by Van der Waals forces and plausible π–π interactions between the aromatic structure of MB and the carbon-based matrix of SMCDA. Additionally, at alkaline pH, Si–OH functional groups enhance MB uptake by generating a negative charge, and calcium species participate through surface complexation and ion exchange, thereby increasing the effectiveness of MB adsorption.

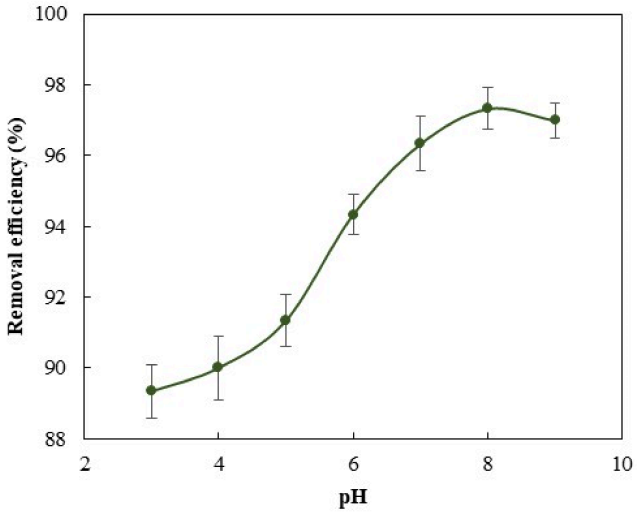


Figure 6. Effect of solution pH on MB removal by SMCDA (Experimental conditions: SMCDA dosage = 1000 mg L^{-1}, initial MB concentration = 15 μM, adsorption time = 4 h, including initial 0.5 h stirring at 700 rpm).

3.8. Effect of Temperature

The adsorption of MB dye is studied in the temperature range of 8–30 °C at an initial MB concentration of 15 μM (Figure 7) and an SMCDA of 1000 mg L^{-1} at equilibrium time. The findings reveal improved MB removal efficacy as temperature increases. Higher temperature promotes interactions between MB molecules and the active sites of SMCDA, as well as MB diffusion. Cattle manure biochar exhibits a similar trend, with higher temperature leading to a stronger adsorption response [21]. Between 25 and 30 °C, the temperature effect on MB removal is insignificant, indicating that SMCDA can be implemented for wastewater treatment at room temperature. The temperature result is discussed to show an operational trend.

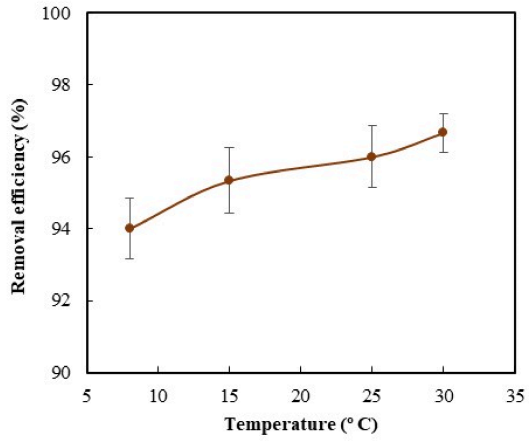


Figure 7. Effect of temperature on MB removal by SMCDA (Experimental conditions: SMCDA dosage = 1000 mg L^{-1}, initial MB concentration under natural pH condition = 15 μM, adsorption time = 4 h, including initial 0.5 h stirring at 700 rpm).

4. Adsorption Isotherm

Statistical analyses reveal distinct variations in model performance. The MOORA ranking method is used to objectively rank the models. For the MOORA, the decision matrix (Table S4) is first constructed using statistical indicators derived from each isotherm model. The matrix is normalized to ensure all criteria are comparable (Table S5). R^2 is considered a beneficial criterion because a higher value indicates better model performance. RMSE, AICc, BIC, HQC, AF, and $|BF-1|$ are considered non-beneficial criteria because lower values indicate lower error or lower model penalty. The final MOORA score is calculated by subtracting the sum of normalized non-beneficial criteria from the sum of normalized beneficial criteria (Table S6). The model with the highest final score is ranked first, as shown in Table 3. The results show that the Freundlich model ranks highest (Y_i: 0.07481). The MOORA analysis is used as a supplementary multi-criteria technique for comparing the isotherm models. According to MOORA, Temkin has the lowest rank (Y_i: −0.31082). Small differences in MOORA scores, particularly between three-parameter models, should, however, not be over-interpreted. Interpretation of the final model is based on statistical performance, simplicity, the plausibility of the parameters, and physical meaning. The analysis supports the Freundlich model as the most accurate representation of MB adsorption on SMCDA. The model highlights the heterogeneous nature of the adsorbent surface. The Freundlich isotherm constant is K_F, and a heterogeneous system is indicated by a small $1/n_F$ value [54–56]. It is observed that the value of n_F lies between 1 and 10, confirming favorable adsorption of MB ions onto the adsorbent used [57]. The Freundlich model provides an equilibrium adsorption capacity of 13.944 mg g^{-1} at the highest experimentally investigated concentration, which is close to the experimental value of 14.425 mg g^{-1}. Details of all seven isotherm fitted parameters are presented in Table S7.

Table 3. Extended MOORA ranking of isotherm models.

Model	Σ Beneficiary	Σ Non-Beneficiary	Y_i (MOORA Index)	Rank
Freundlich	0.05575	−0.01907	0.07481	1
Sips	0.05573	0.09276	−0.03703	2
Toth	0.05537	0.15038	−0.09501	3
Langmuir	0.05333	0.28563	−0.23230	4
Unilan	0.05403	0.31556	−0.26153	5
Jovanovic	0.05265	0.35545	−0.30280	6
Temkin	0.05092	0.36174	−0.31082	7

5. Mechanism

SMCDA shows improved MB adsorption owing to its hierarchical macro/mesoporous structure and amount of oxygen-containing functional groups. The feasible adsorption mechanism includes electrostatic attraction between the negatively charged SMCDA surface and cationic MB molecules, with possible π-π interactions between the aromatic ring of the carbon and MB (Figure 8). The measured zeta potential of SMCDA is −26.90 mV, indicating a negatively charged surface with plausible electrostatic attraction with cationic MB molecules. However, the zeta potential is determined only at the suspension's natural pH; no conclusions can be drawn regarding the surface charge behavior over the entire pH range (3–9) investigated in the adsorption experiments. These synergistic mechanisms account for the substantial adsorption capacity and efficient removal of MB from the aqueous solution. BET analysis confirms that the SMCDA possesses a specific surface area of 9.197 m^2 g^{-1}, a pore volume of 0.030 cm^3 g^{-1}, and an average pore diameter of 13.23 nm (mesopores). However, SEM images show macro pores. Therefore, the SMCDA

has a hierarchical macro/mesoporous structure that enables the removal of MB molecules. The FTIR spectra of SMCDA after MB removal is shown in Figure S1. FTIR comparison of SMCDA before and after treatment shows that the hydrogen-bonded O-H peak changed from 3500 to 3462.56 cm^{-1}, suggesting that surface hydroxyl groups are participating in hydrogen bonding and electrostatic interactions with MB molecules. The band at 1656 cm^{-1} changes to 1635.34 cm^{-1}, revealing interactions between the SMCDA and MB.

Additionally, the Si–O–Si/Si–O–Al stretching band moves from 1095 to 1050 cm^{-1}, suggesting that surface interactions within the aluminosilicate framework contributed to the MB removal. Modifications in peaks after MB adsorption further suggest the elimination of the bands at 1440 and 823 cm^{-1} and the emergence of a new band at 785.47 cm^{-1}. The new band is consistent with the possibility of MB removal, which relates to vibrations associated with the aromatic phenothiazine ring of deposited MB.

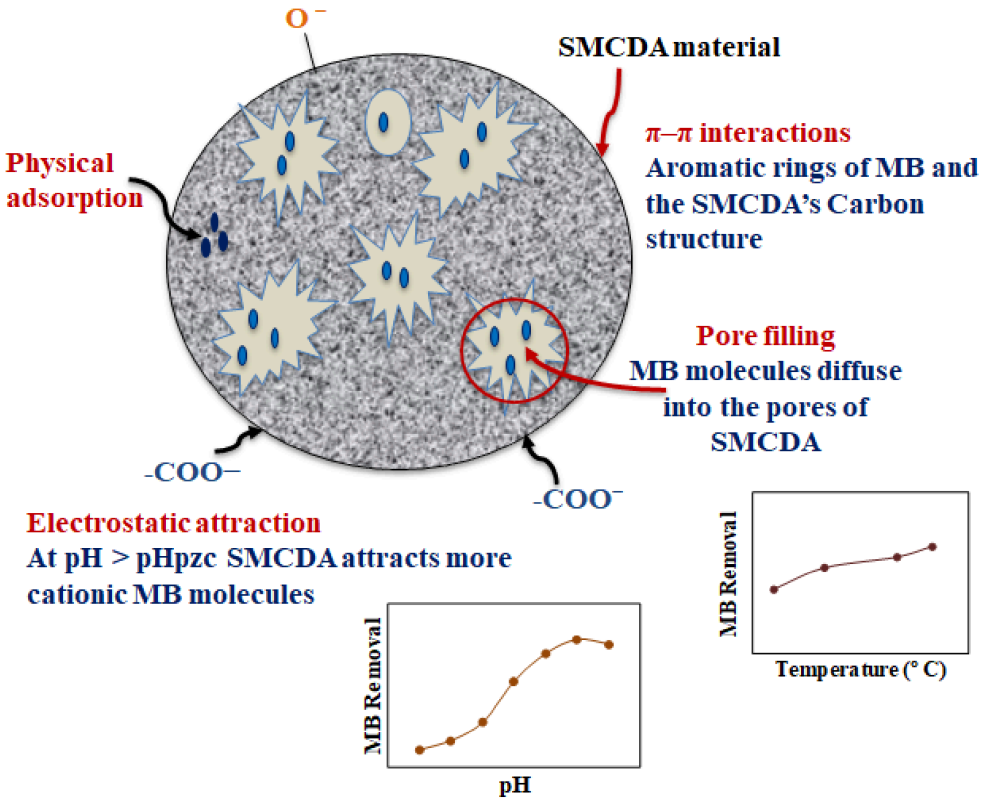


Figure 8. Mechanism of MB removal by SMCDA.

6. Conclusions

This study demonstrates that SMCDA is a viable adsorbent for removing MB from water. The observed adsorption performance demonstrates the potential of cow dung ash to be valorized as a low-cost alternative adsorbent for wastewater treatment. The static Coulombic interaction between the MB and the SMCDA surface is the main factor responsible for the maximum MB adsorption efficiency of 97.33% at a dosage of 1000 mg L^{-1} and an optimum pH of 8. Results show that an increase in temperature improves the MB adsorption. MOORA shows that the Freundlich isotherm model provides the best fit, predicting an equilibrium adsorption capacity of 13.944 mg g^{-1} at the highest experimentally investigated concentration, which is close to the experimental value of 14.425 mg g^{-1}. This study shows that cow dung can be effectively transformed into an efficient adsorbent for MB removal without using hazardous chemical activating agents, thereby advancing sustainability goals. The suggested method eliminates the use of hazardous chemicals, thereby minimizing environmental impacts, even though its MB uptake

capacity is lower than that of conventionally activated cow dung-derived adsorbents. However, it is crucial to recognize that these findings are from batch experiments with synthetic dye solutions, and the adsorption behavior might differ in more complex wastewater settings. Future research should focus on the regeneration and reuse of the adsorbent, the treatment of real industrial wastewater, and the adoption of continuous-flow systems to evaluate the sustained effectiveness of SMCDA. Thus, this work lays the foundation for future studies to assess the cyclic performance of SMCDA using appropriate regeneration methods.

Supplementary Materials: The following supporting information can be downloaded at: https://www.mdpi.com/article/10.3390/su18168310/s1, Table S1. Experimental (q_e exp.) and model-calculated (q_e cal.) adsorbed concentrations. Table S2. Goodness of fit statistics and fitted kinetic parameters of PFO and PSO models. Table S3. Predicted values of q_e (mg g^{-1}) by seven isotherm models. Table S4. Decision Matrix for MOORA analysis. Table S5. Vector normalized Matrix for MOORA analysis. Table S6. Weighted-Normalized Matrix for MOORA analysis. Table S7. Details of adsorption isotherm model parameters. Figure S1. FTIR spectrum of SMCDA after MB adsorption.

Author Contributions: Conceptualization, V.R.C., N.A.D. and R.M.K.; methodology, V.R.C., N.A.D. and R.M.K.; software, Y.S.; validation, R.M.K., G.R.C. and M.S.; formal analysis, R.M.K., G.R.C. and Y.S.; investigation, V.R.C., N.A.D. and R.M.K.; resources, G.R.C.; data curation, N.A.D., R.M.K. and Y.S.; writing—original draft preparation, V.R.C., N.A.D. and R.M.K.; writing—review and editing, G.R.C., Y.S. and M.S.; visualization, G.R.C., Y.S. and M.S.; supervision, R.M.K.; All authors have read and agreed to the published version of the manuscript.

Funding: This research received no external funding.

Institutional Review Board Statement: Not applicable.

Informed Consent Statement: Not applicable.

Data Availability Statement: The authors confirm that all the data supporting the findings of this study are available within the article.

Acknowledgments: We are thankful to DST-FIST Analytical Instrumentation Laboratory at Jaysingpur College, Jaysingpur, and Shivaji University, Kolhapur, Maharashtra, India, for supporting the material characterization.

Conflicts of Interest: The authors declare no conflicts of interest.

References

1. Hongo, T.; Moriura, M.; Hatada, Y.; Abiko, H. Simultaneous Methylene Blue Adsorption and pH Neutralization of Contaminated Water by Rice Husk Ash. *ACS Omega* **2021**, *6*, 21604–21612. [CrossRef]
2. Akter, T.; Protity, A.T.; Shaha, M.; Al Mamun, M.; Hashem, A. The Impact of Textile Dyes on the Environment. In *Nanohybrid Materials for Treatment of Textiles Dyes*; Springer: Singapore, 2023; pp. 401–431. [CrossRef]
3. Huan, Y.; Wang, G.; Li, C.; Li, G. Acrylic acid grafted-multi-walled carbon nanotubes and their high-efficiency adsorption of methylene blue. *J. Mater. Sci.* **2020**, *55*, 4656–4670. [CrossRef]
4. Chate, V.R.; Kulkarni, R.M.; Mutalik Desai, V.G.; Kunkangar, P.B. Seawater-Washed Activated Bauxite Residue for Fluoride Removal: Waste Utilization Technique. *J. Environ. Eng.* **2018**, *144*, 04018031. [CrossRef]
5. Ma, J.; Yu, F.; Zhou, L.; Jin, L.; Yang, M.; Luan, J.; Tang, Y.; Fan, H.; Yuan, Z.; Chen, J. Enhanced Adsorptive Removal of Methyl Orange and Methylene Blue from Aqueous Solution by Alkali-Activated Multiwalled Carbon Nanotubes. *ACS Appl. Mater. Interfaces* **2012**, *4*, 5749–5760. [CrossRef] [PubMed]
6. Mishra, A.; Mehta, A.; Sharma, M.; Basu, S. Enhanced heterogeneous photodegradation of VOC and dye using microwave synthesized TiO2/Clay nanocomposites: A comparison study of different type of clays. *J. Alloys Compd.* **2017**, *694*, 574–580. [CrossRef]
7. Zheng, S.; Guo, H.; Yang, F.; Hong, B. Novel organic dye sorbent: Synthesis and adsorption properties of multi-walled carbon nanotubes modified with gallic amide units. *Desalin. Water Treat.* **2016**, *57*, 12264–12273. [CrossRef]

8. Arora, C.; Soni, S.; Sahu, S.; Mittal, J.; Kumar, P.; Bajpai, P.K. Iron based metal organic framework for efficient removal of methylene blue dye from industrial waste. *J. Mol. Liq.* **2019**, *284*, 343–352. [CrossRef]
9. Al-Tohamy, R.; Ali, S.S.; Li, F.; Okasha, K.M.; Mahmoud, Y.A.-G.; Elsamahy, T.; Jiao, H.; Fu, Y.; Sun, J. A critical review on the treatment of dye-containing wastewater: Ecotoxicological and health concerns of textile dyes and possible remediation approaches for environmental safety. *Ecotoxicol. Environ. Saf.* **2022**, *231*, 113160. [CrossRef] [PubMed]
10. Din, M.I.; Khalid, R.; Najeeb, J.; Hussain, Z. Fundamentals and photocatalysis of methylene blue dye using various nanocatalytic assemblies- a critical review. *J. Clean. Prod.* **2021**, *298*, 126567. [CrossRef]
11. Mouni, L.; Belkhiri, L.; Bollinger, J.-C.; Bouzaza, A.; Assadi, A.; Tirri, A.; Dahmoune, F.; Madani, K.; Remini, H. Removal of Methylene Blue from aqueous solutions by adsorption on Kaolin: Kinetic and equilibrium studies. *Appl. Clay Sci.* **2018**, *153*, 38–45. [CrossRef]
12. Misran, E.; Bani, O.; Situmeang, E.M.; Purba, A.S. Removal efficiency of methylene blue using activated carbon from waste banana stem: Study on pH influence. *IOP Conf. Ser. Earth Environ. Sci.* **2018**, *122*, 012085. [CrossRef]
13. Chauhan, R.; Kumar, A.; Chaudhary, R.P. Photocatalytic degradation of methylene blue with Cu doped ZnS nanoparticles. *J. Lumin.* **2014**, *145*, 6–12. [CrossRef]
14. Rafatullah, M.; Sulaiman, O.; Hashim, R.; Ahmad, A. Adsorption of methylene blue on low-cost adsorbents: A review. *J. Hazard. Mater.* **2010**, *177*, 70–80. [CrossRef] [PubMed]
15. Özer, A.; Toprak, M. Highly efficient removal of methylene blue from aqueous solution by magnetic biochar prepared from hawthorn seeds. *Environ. Prog. Sustain. Energy* **2023**, *42*, e14127. [CrossRef]
16. Jagtap, S.; Yenkie, M.K.; Labhsetwar, N.; Rayalu, S. Fluoride in Drinking Water and Defluoridation of Water. *Chem. Rev.* **2012**, *112*, 2454–2466. [CrossRef] [PubMed]
17. Tang, Q.; Shi, C.; Shi, W.; Huang, X.; Ye, Y.; Jiang, W.; Kang, J.; Liu, D.; Ren, Y.; Li, D. Preferable phosphate removal by nano-La(III) hydroxides modified mesoporous rice husk biochars: Role of the host pore structure and point of zero charge. *Sci. Total Environ.* **2019**, *662*, 511–520. [CrossRef] [PubMed]
18. Saud, A.; Gupta, S.; Allal, A.; Preud'homme, H.; Shomar, B.; Zaidi, S.J. Progress in the Sustainable Development of Biobased (Nano)materials for Application in Water Treatment Technologies. *ACS Omega* **2024**, *9*, 29088–29113. [CrossRef] [PubMed]
19. Li, Y.-H.; Wang, S.; Zhang, X.; Wei, J.; Xu, C.; Luan, Z.; Wu, D. Adsorption of fluoride from water by aligned carbon nanotubes. *Mater. Res. Bull.* **2003**, *38*, 469–476. [CrossRef]
20. Jiang, D.; Li, H.; Cheng, X.; Ling, Q.; Chen, H.; Barati, B.; Yao, Q.; Abomohra, A.; Hu, X.; Bartocci, P.; et al. A mechanism study of methylene blue adsorption on seaweed biomass derived carbon: From macroscopic to microscopic scale. *Process Saf. Environ. Prot.* **2023**, *172*, 1132–1143. [CrossRef]
21. Zhu, Y.; Yi, B.; Yuan, Q.; Wu, Y.; Wang, M.; Yan, S. Removal of methylene blue from aqueous solution by cattle manure-derived low temperature biochar. *RSC Adv.* **2018**, *8*, 19917–19929. [CrossRef] [PubMed]
22. Quansah, J.O.; Hlaing, T.; Lyonga, F.N.; Kyi, P.P.; Hong, S.-H.; Lee, C.-G.; Park, S.-J. Nascent Rice Husk as an Adsorbent for Removing Cationic Dyes from Textile Wastewater. *Appl. Sci.* **2020**, *10*, 3437. [CrossRef]
23. Halysh, V.; Sevastyanova, O.; Pikus, S.; Dobele, G.; Pasalskiy, B.; Gun'ko, V.M.; Kartel, M. Sugarcane bagasse and straw as low-cost lignocellulosic sorbents for the removal of dyes and metal ions from water. *Cellulose* **2020**, *27*, 8181–8197. [CrossRef]
24. Ogundiran, A.A.; Ogundiran, O.O.; Adejoke, B.A.; El Gamal, A.; Bin Emran, T.; Hefnawy, M. Sustainable wastewater treatment: Raw and activated cow dung for the sorption of methylene blue dye. *BioResources* **2025**, *20*, 6815–6836. [CrossRef]
25. Ho, Y. Review of second-order models for adsorption systems. *J. Hazard. Mater.* **2006**, *136*, 681–689. [CrossRef] [PubMed]
26. Lyu, F.; Niu, S.; Wang, L.; Liu, R.; Sun, W.; He, D. Efficient removal of Pb(II) ions from aqueous solution by modified red mud. *J. Hazard. Mater.* **2021**, *406*, 124678. [CrossRef] [PubMed]
27. Chu, K.H.; Hashim, M.A.; Debord, J.; Harel, M.; Salvestrini, S.; Bollinger, J.-C. The Jovanović adsorption isotherm in water contaminant research: Unmasking spurious versions and spotlighting the real thing. *Chem. Eng. Sci.* **2023**, *281*, 119127. [CrossRef]
28. Carmo, A.M.; Hundal, L.S.; Thompson, M.L. Sorption of Hydrophobic Organic Compounds by Soil Materials: Application of Unit Equivalent Freundlich Coefficients. *Environ. Sci. Technol.* **2000**, *34*, 4363–4369. [CrossRef]
29. Sánchez-Moreno, H.; García-Rodríguez, L.; Recalde-Moreno, C. Natural cellulose fibers from *Agave americana* L. ASPARAGACEAE as an effective adsorbent for mercury in aqueous solutions. *Adsorption* **2025**, *31*, 40. [CrossRef]
30. Murphy, O.P.; Vashishtha, M.; Palanisamy, P.; Kumar, K.V. A Review on the Adsorption Isotherms and Design Calculations for the Optimization of Adsorbent Mass and Contact Time. *ACS Omega* **2023**, *8*, 17407–17430. [CrossRef] [PubMed]
31. Mayer, F.; Rehner, P.; Seiler, J.; Schilling, J.; Gross, J.; Bardow, A. Adsorption Modeling Based on Classical Density Functional Theory and PC-SAFT: Temperature Extrapolation and Fluid Transfer. *Ind. Eng. Chem. Res.* **2024**, *63*, 14137–14147. [CrossRef] [PubMed]
32. Bhadra, S.J.; Ebner, A.D.; Ritter, J.A. On the Use of the Dual Process Langmuir Model for Predicting Unary and Binary Isosteric Heats of Adsorption. *Langmuir* **2012**, *28*, 6935–6941. [CrossRef] [PubMed]

33. Subramanyam, B.; Das, A. Linearised and non-linearised isotherm models optimization analysis by error functions and statistical means. *J. Environ. Health Sci. Eng.* **2014**, *12*, 92. [CrossRef] [PubMed]
34. Vareda, J.P. On validity, physical meaning, mechanism insights and regression of adsorption kinetic models. *J. Mol. Liq.* **2023**, *376*, 121416. [CrossRef]
35. Burnham, K.P.; Anderson, D.R. Multimodel Inference. *Sociol. Methods Res.* **2004**, *33*, 261–304. [CrossRef]
36. López, S.; Prieto, M.; Dijkstra, J.; Dhanoa, M.S.; France, J. Statistical evaluation of mathematical models for microbial growth. *Int. J. Food Microbiol.* **2004**, *96*, 289–300. [CrossRef] [PubMed]
37. Ye, K.; Wang, H.; Zhang, X.; Jiang, Y.; Xu, X.; Zhou, G. Development and validation of a molecular predictive model to describe the growth of *Listeria monocytogenes* in vacuum-packaged chilled pork. *Food Control* **2013**, *32*, 246–254. [CrossRef]
38. Baty, F.; Ritz, C.; Charles, S.; Brutsche, M.; Flandrois, J.-P.; Delignette-Muller, M.-L. A Toolbox for Nonlinear Regression in R: The Package nlstools. *J. Stat. Softw.* **2015**, *66*, 1–21. [CrossRef]
39. Sarstedt, M.; Hair, J.F.; Pick, M.; Liengaard, B.D.; Radomir, L.; Ringle, C.M. Progress in partial least squares structural equation modeling use in marketing research in the last decade. *Psychol. Mark.* **2022**, *39*, 1035–1064. [CrossRef]
40. Chakraborty, S. Applications of the MOORA method for decision making in manufacturing environment. *Int. J. Adv. Manuf. Technol.* **2011**, *54*, 1155–1166. [CrossRef]
41. Karande, P.; Chakraborty, S. Application of multi-objective optimization on the basis of ratio analysis (MOORA) method for materials selection. *Mater. Des.* **2012**, *37*, 317–324. [CrossRef]
42. Singh, R.; Pathak, V.K.; Kumar, R.; Dikshit, M.; Aherwar, A.; Singh, V.; Singh, T. A historical review and analysis on MOORA and its fuzzy extensions for different applications. *Heliyon* **2024**, *10*, e25453. [CrossRef] [PubMed]
43. Mardani, A.; Jusoh, A.; Md Nor, K.; Khalifah, Z.; Zakwan, N.; Valipour, A. Multiple criteria decision-making techniques and their applications—A review of the literature from 2000 to 2014. *Econ. Res. Istraž.* **2015**, *28*, 516–571. [CrossRef]
44. Shukor, M.Y. Chitosan–Silica Composite Aerogel for the Adsorption of Cupric Ions: Isothermal Remodeling and MOORA-Based Model Selection. *J. Environ. Microbiol. Toxicol.* **2024**, *12*, 53–62. [CrossRef]
45. Sadiq, M.; Aman, R.; Hussain, S.; Zia, M.A.; Rahman, N.U.; Saeed, M. Green and Efficient Oxidation of Octanol by Iron Oxide Nanoparticles Supported on Activated Carbon. *Mod. Res. Catal.* **2015**, *04*, 28–35. [CrossRef]
46. Murugan, K.; Nataraj, D.; Madhiyazhagan, P.; Sujitha, V.; Chandramohan, B.; Panneerselvam, C.; Dinesh, D.; Chandirasekar, R.; Kovendan, K.; Suresh, U.; et al. Carbon and silver nanoparticles in the fight against the filariasis vector *Culex quinquefasciatus*: Genotoxicity and impact on behavioral traits of non-target aquatic organisms. *Parasitol. Res.* **2016**, *115*, 1071–1083. [CrossRef] [PubMed]
47. Qiu, X.; Wang, L.; Zhu, H.; Guan, Y.; Zhang, Q. Lightweight and efficient microwave absorbing materials based on walnut shell-derived nano-porous carbon. *Nanoscale* **2017**, *9*, 7408–7418. [CrossRef] [PubMed]
48. Xie, X.; Wu, D.; Wu, H.; Hou, C.; Sun, X.; Zhang, Y.; Yu, R.; Zhang, S.; Wang, B.; Du, W. Dielectric parameters of activated carbon derived from rosewood and corncob. *J. Mater. Sci. Mater. Electron.* **2020**, *31*, 18077–18084. [CrossRef]
49. Nang An, V.; Van, T.T.T.; Nhan, H.T.C.; Van Hieu, L. Investigating Methylene Blue Adsorption and Photocatalytic Activity of ZnO/CNC Nanohybrids. *J. Nanomater.* **2020**, *2020*, 6185976. [CrossRef]
50. Liang, Y.; Ouyang, J.; Wang, H.; Wang, W.; Chui, P.; Sun, K. Synthesis and characterization of core–shell structured SiO2@YVO4:Yb3+,Er3+ microspheres. *Appl. Surf. Sci.* **2012**, *258*, 3689–3694. [CrossRef]
51. Marshall, J.A.; Morton, B.J.; Muhlack, R.; Chittleborough, D.; Kwong, C.W. Recovery of phosphate from calcium-containing aqueous solution resulting from biochar-induced calcium phosphate precipitation. *J. Clean. Prod.* **2017**, *165*, 27–35. [CrossRef]
52. Kaur, K.; Mor, S.; Ravindra, K. Removal of chemical oxygen demand from landfill leachate using cow-dung ash as a low-cost adsorbent. *J. Colloid Interface Sci.* **2016**, *469*, 338–343. [CrossRef] [PubMed]
53. Li, J.Q.S.; Wang, H.; Wang, Y.Q. Preparation of Silica/Polymer Hybrid Nanoparticles via a Semi-Continuous Soup-Free Emulsion Polymerization. *Adv. Mater. Res.* **2015**, *1120–1121*, 233–242. [CrossRef]
54. Rushton, G.T.; Karns, C.L.; Shimizu, K.D. A critical examination of the use of the Freundlich isotherm in characterizing molecularly imprinted polymers (MIPs). *Anal. Chim. Acta* **2005**, *528*, 107–113. [CrossRef]
55. Liu, Y.; Liu, Y.-J. Biosorption isotherms, kinetics and thermodynamics. *Sep. Purif. Technol.* **2008**, *61*, 229–242. [CrossRef]
56. Ayawei, N.; Ebelegi, A.N.; Wankasi, D. Modelling and Interpretation of Adsorption Isotherms. *J. Chem.* **2017**, *2017*, 3039817. [CrossRef]
57. Yakkerimath, S.; Kulkarni, R.M.; Divekar, S.V.; Chate, V.R.; Bekal, K.P. Kinetic, adsorption, and thermodynamic study of removal of Cr6+ by iron-rich natural clay minerals. *Desalin. Water Treat.* **2024**, *318*, 100302. [CrossRef]

Disclaimer/Publisher's Note: The statements, opinions and data contained in all publications are solely those of the individual author(s) and contributor(s) and not of MDPI and/or the editor(s). MDPI and/or the editor(s) disclaim responsibility for any injury to people or property resulting from any ideas, methods, instructions or products referred to in the content.